Journal of Engineering and Science Research 6 (5): 50-61, 2022
e-ISSN: 2289-7127

DOI: 10.26666/rmp.jesr.2022.5.6

Analysis of Wake Interaction of Savonius Tidal Turbine in Shallow Water Application

Syahfiq Misran[a], Anas Abdul Rahman[a], Ayu Abdul-Rahman[b], Azzim Rosli[a], Wan Muhammad Fadhli Arif[a] , Ramadhan Ahmed Ramadhan Basiddiq[a] , Najwa Syafiqa Marzuki[a]

[a]Mechanical Engineering Program, Faculty of Mechanical Engineering Technology, Universiti Malaysia Perlis, Pauh Putra Main Campus, 02600 Perlis, Malaysia.
[b]Department of Mathematics and Statistics, School of Quantitative Sciences, Universiti Utara Malaysia, 06010 UUM, Sintok, Kedah, Malaysia

Received: 10 August 2022; Revised: 03 September 2022; Accepted: 10 October 2022; Published: 30 October 2022

Abstract: Malaysia highly depends on non-renewable energy sources like fossil fuels to supply the country's growing energy needs. On the other side, the oil and gas industry is facing challenges due to the depletion of fossil fuel supplies. Renewable energy is an alternative to fossil fuels that has been developed as a means of maintaining steady development in Malaysia. This is due to the slow average current speed in the sea around the country. Various renewable energy sources have been researched, with tidal energy garnering the most interest. This study focuses on tidal turbine array configuration for shallow water applications by using a Savonius turbine. The turbine layout is challenging to deploy the tidal array properly, and the wake interaction between the devices must be studied. The multi-row and single-row arrays have been studied using Computational Fluid Dynamics (CFD) simulations. The numerical research using a CFD technique is used to explore the effect of turbine spacing and capacity on the array's wake production. The vertical axis turbine is represented by a hypothetical 'actuator' cylinder and a 'Savonius' disc (VATT). Following the domain configuration, the turbine has been configured to static modes. According to the findings, the VATT model has a faster wake recovery and follows the definition of the distant wake. When working in shallow water, staggered arrays with bigger spacing are recommended since there is a lower chance of wake mixing between the rows.

Keywords: *Marine renewable energy, Computational fluid dynamic, Vertical axis tidal turbine, Grid sensitivity study, Array configurations*

INTRODUCTION

More than 90% of power generation in Malaysia is dependent on fossil fuels. Thus, the constant expansion in energy demand has contributed to an increase in CO_2 emissions [1][2]. Due to emission control, greenhouse gas and fossil fuel exploitation methods, the use of renewable energy to replace fossil fuels reduces detrimental environmental and ecological repercussions. As a result, to assure sustainable power development and promote energy transition, important and far-reaching initiatives in renewable energy generation must be made [3]. One of the most exciting breakthroughs in recent years to prevent climate change has been the energy shift from conventional to clean energy sources, namely renewable energy. However, energy system transition has an impact on economic policy agendas, and policymakers

Corresponding Author: Anas Abdul Rahman, Mechanical Engineering Program, Faculty of Mechanical Engineering Technology, Universiti Malaysia Perlis, Pauh Putra Main Campus, 02600 Arau, Perlis, Malaysia, anasrahman@unimap.edu.my

throughout the world are looking for ways to spread clean energy and alter energy systems [4]. Malaysia is aiming for a 31% renewable energy capacity by 2025, according to the Malaysia Investment Development Authority (MIDA). Figure 1 shows Malaysia's generation capacity of total electrical. Malaysia intends to boost its renewable energy installed capacity to 31% in 2025 and 40% in 2035. Peninsular Malaysia will be the focus of the Malaysian government's efforts to enhance renewable energy in the country's power capacity mix since it accounts for 80% of the country's electricity consumption. Malaysia's energy transition strategy should be cost-effective, in line with Sustainable Development Goal 7 of ensuring access to affordable, reliable, sustainable, and modern energy for all [5].

Tidal energy is an essential renewable energy source, but it is also one of the best energies of renewable energy that can be applied in Malaysia. There is a lack of interest and study in tidal energy in Malaysia compared to other renewable sources such as solar, wind, and hydro. Tidal power facilities can survive up to four times as long as wind or solar farms [6]. Compared with the Horizontal Axis Tidal Turbine (HATT), research and development of the VATT lag because of the complex flow structure and periodic unsteady separation flow.

According to a survey of the literature, the average current velocity in Malaysian seas is 1 m/s. Although velocities surpassing 1.5 m/s have been documented at some places, this is generally regarded as too low for a sustainable tidal stream power production. The problem is Malaysia's seawater condition has a low current velocity [7]. It will have difficulty for the tidal turbine system to generate electricity. The presence of wind waves increases the turbulent complexity of the flow, changes the dynamic behaviour of the tidal-stream turbine, and adds to the performance and survivability issues [8]. The purpose of this project is to investigate the Savonius tidal turbine wake interaction in shallow water via the CFD simulation.

There was an early surge of interest in renewable energy choices in response to the oil crisis of that time, which led to the development of tidal energy systems that have been around since then. Figure 2 shows how tidal energy is extracted from the ocean. As the world is now experiencing the effects of climax change, such as prolonged draught and melting glaciers, various pledges such as Net Zero 2030 are a welcome commitment by nations around the world to limit the damage done to the environment due to the uncontrol use of hydrocarbons [9].

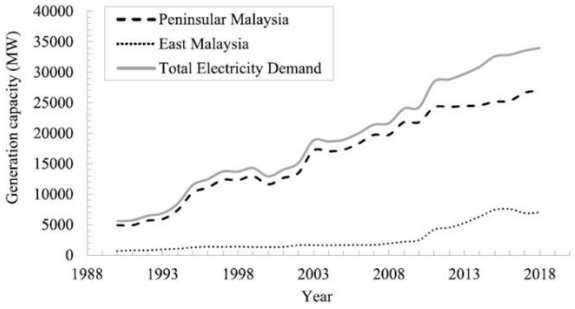

Fig 1 Malaysia's generation capacity [10]

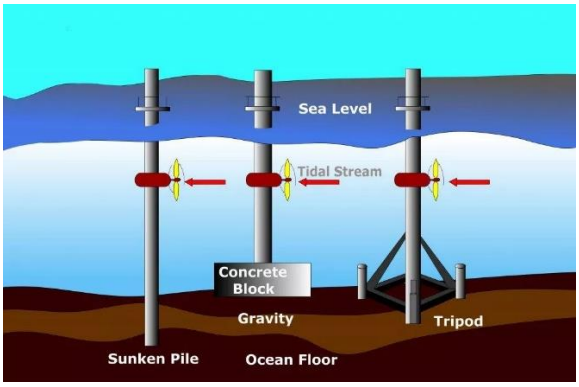

Fig 2 Tidal energy process diagram [11]

SIMULATION

Modelling

Table 1 The parameters of the Savonius turbine and domain specification

Savonius Turbine Parameters	
Model Parameters	**Dimension (m)**
Rotor Height, H	5.00
Rotor Diameter, D	2.50
Shaft Diameter, a	0.15
Overlap, e	0.30
Blade Diameter, d	1.25
Blade Thickness	0.05
End Plate Thickness	0.10
Domain specification	
Depth	30m
Width	80m
Length	800m
Turbine positioning	62.5m

The study begins with a review of past instances in order to gather relevant information and a brief explanation of the processes followed to complete and achieve the research's objectives. The VATT is selected in numerical modelling because of its rapid simulation and easier meshing procedure than other methods of numerical modelling, according to most research investigations. This section also offers a brief overview of the methods used to attain the research objectives. To construct a Savonius Tidal Turbine, a few parameters must be considered. The size and geometrical form of the turbine are among them. The specified parameters are important since they have an impact on the meshing quality prior to the CFD simulation. The meshing quality is crucial since it has an impact on the simulation results. After the CAD model was meshed, fluent analysis was then utilized to stimulate it. Before finishing the simulation research, several factors should be examined, including the flow velocity at 0.6 m/s, clearance at the top and bottom of the turbine, and domain dimensions. In the last phases, the data from the actuator cylinder and the Savonius Tidal Turbine have been compared and validated. Figure 3 shows the geometry parameter for the Savonius turbine in the front and top view. Table 1 shows the parameters of the Savonius turbine in meters

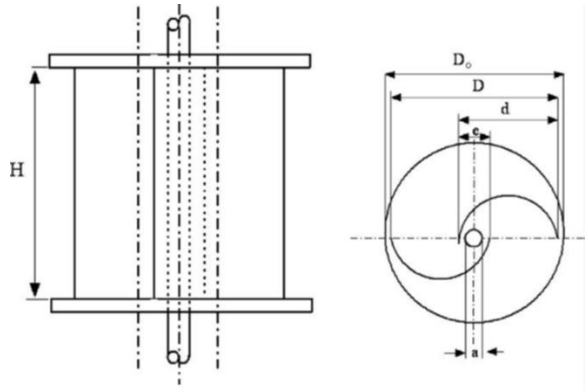

Fig 3 Geometry parameter for Savonius turbine, (a) Front view; (b) Top view

Table 2 Array Parameter

Parameter	Lateral spacing (m)	Longitudinal spacing (m)
Inline	1.5D	-
Staggered		4D

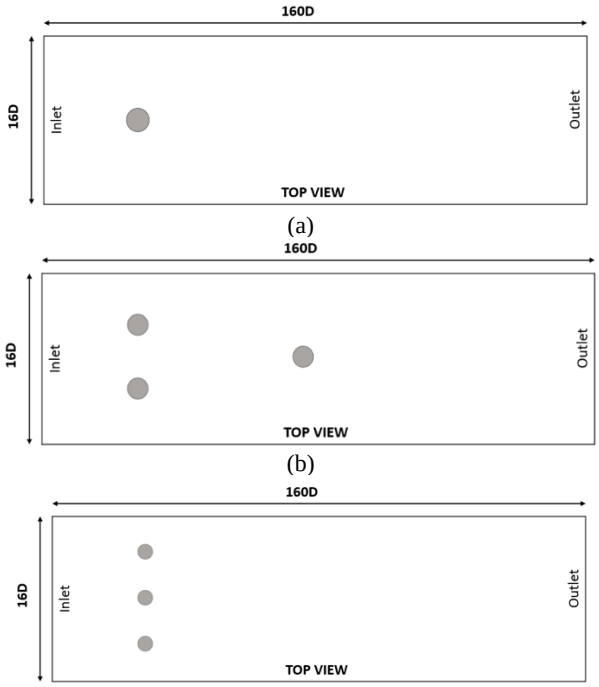

Fig 4 Domain Setup. (a) Configuration A domain setup; (b) Configuration B domain setup; (c) Configuration C domain setup.

This study's boundary conditions, which have been used to define the domain, are based on the work of Gisrina Elin Suhairi [12]. A mean water temperature of 27°C has been used to determine the density of seawater and the dynamic viscosity of 0.00092 Ns/m³ following that. There are two separate current velocity values; 1.0m/s water current and 0.6 m/s average water current.

The investigation was carried out utilizing several Savonius turbine designs, including configuration A (single setup), configuration B (staggered setup), and configuration C (inline setup), with precise spacing as listed in Table 2. This is shown in Figs. 4 (a)-(c).

Mesh Independence Study

Table 3 illustrates the unstructured tetra-mesh generated by Ansys Fluent with 5 different domain element sizes for each turbulence model. The faces of the turbine were also subjected to mesh refining. The mesh inflating technique was built using the smooth transition option with a maximum of 5 layers.

Table 3 Grid Sensitivity Study

Refinement	Element size (m)	Nodes	No. of Elements
Very fine	1.5	1,438,495	7,318,499
Fine	2.0	849,350	3,903,471
Medium	2.5	636,284	2,683,487

Coarse	3.0	541,937	2,147,166
Very coarse	3.5	492,345	1,870,536

Table 3 also illustrates how to increase the number of nodes and elements in numerical simulation by decreasing the element size of the domain and turbine faces from extremely coarse to very fine refinement. As a result, the precision and quality of numerical research solutions will improve. Nonetheless, the time it takes to produce a high-quality model has an impact on the pace of the simulation. It has been discovered that meshing with a high order of mesh formation takes the longest time, as does determining the numerical solution for the process of breaking down the continuous geometric space of the domain and faces into smaller forms to suitably mesh together.

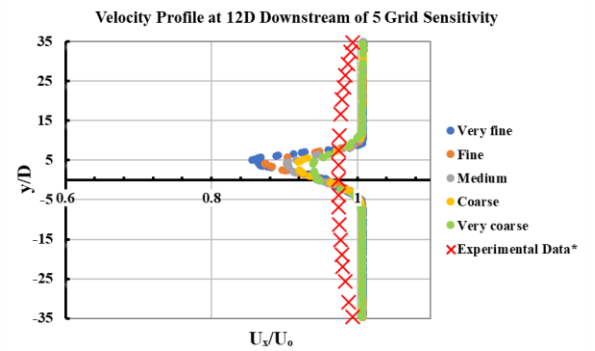

Fig 5 Velocity profile at 12D downstream of 5 grid sensitivity.

Figure 5 depicts the velocity profile at 12D downstream of the Savonius Turbine for each kind of meshing refinement. The figure shows that five alternative meshing modifications, especially the velocity profile at 12D downstream, may duplicate the experimental pattern. This means that the meshing refinement has just a minimal impact on the velocity profile behind the turbine. As a consequence, any meshing refinement may be applied numerically. Grid sensitivity analysis, as shown in Figure 6 provides a fresh viewpoint on meshing refinement options.

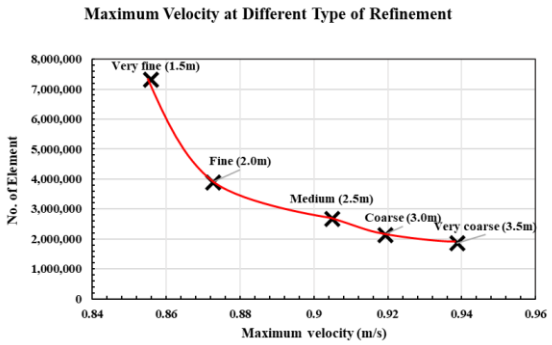

Fig 6 Velocity profile at 12D downstream at different types of refinement.

Table 4 Parameter specification for boundary condition (Type 1-very fine)

Type	Element	Mesh Generation
1	Domain	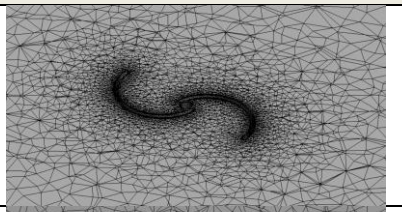
	Faces	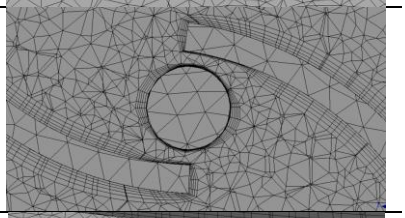
	Edges	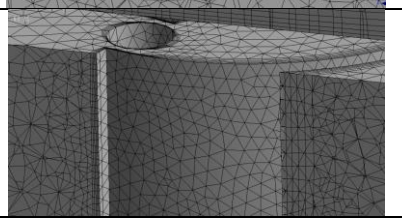

Table 5 Parameter specification for boundary condition (Type 2-fine)

Type	Element	Mesh Generation
2	Domain	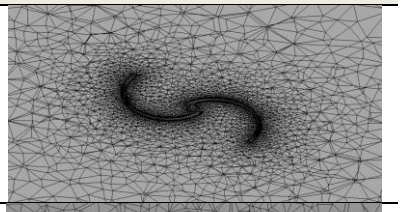
	Faces	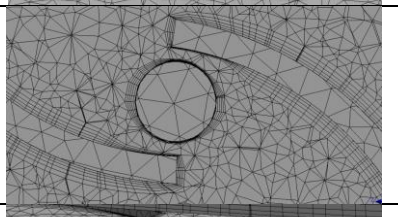
	Edges	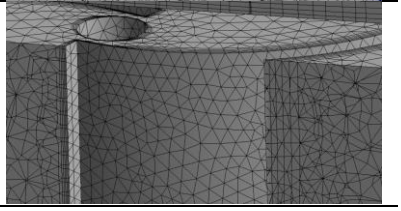

Table 6 Parameter specification for boundary condition (Type 3-Medium)

Type	Element	Mesh Generation
3	Domain	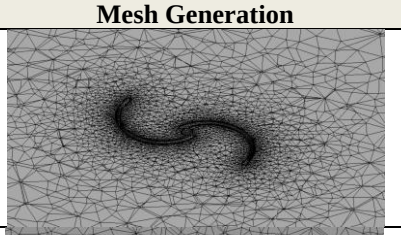
	Faces	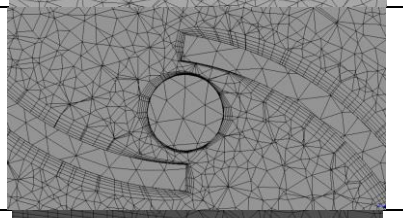
	Edges	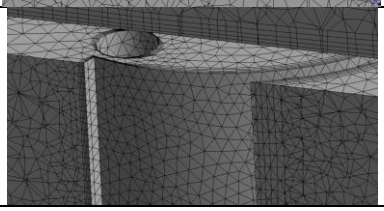

Table 7 Parameter specification for boundary condition (Type 4-Coarse)

Type	Element	Mesh Generation
4	Domain	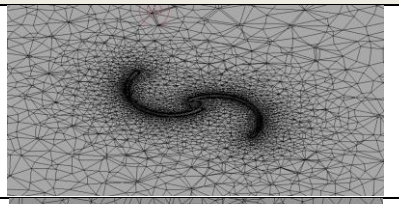
	Faces	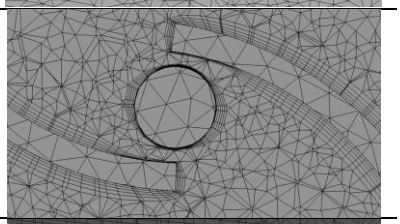
	Edges	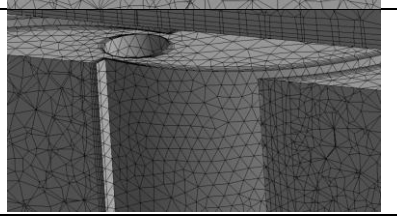

Table 8 Parameter specification for boundary condition (Type 5-Very coarse)

Type	Element	Mesh Generation
5	Domain	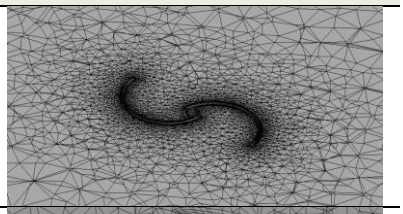
	Faces	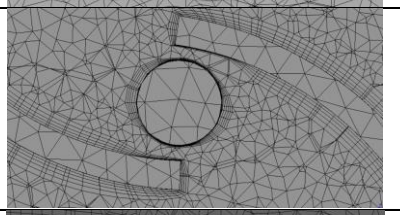
	Edges	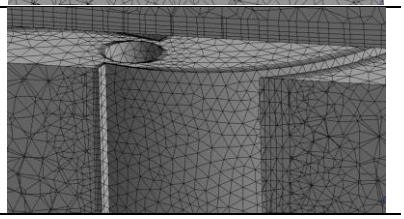

As a result, the optimal alternative for additional numerical calculation and analysis is Type 2 (Fine) meshing refinement. The mesh size, as compared to finer mesh, will give the best results while saving time for numerical computation and analysis. Tables 4 to 8 also show the features of mesh production from different approaches to mesh refining.

CALCULATION

Tidal Stream Energy Conversion Theory

There are several formulas for the tidal stream that may be used to determine the power of a tidal current turbine. The density of both tidal and wind sources using the same equation would be the sole difference. As a result, the power generated by the tidal stream current is [13]

$$P = \frac{1}{2}\rho A v^3 \quad (1)$$

where ρ is the density of the fluid, A is the area of the turbine rotor and *v* is the velocity of the fluid. The HATT and VATT have different cross-sectional areas (A). In the case of VATT, the cross-sectional area will be

$$A = H\ x\ D \quad (2)$$

The VATT will be equal to the height (H) multiplied by the diameter (D) of the rotor. Because of some losses, the tidal current can harvest a part of this power, and the formula can be modified as follows [14]

$$P = \frac{1}{2} C_p \rho A v^3 \quad (3)$$

where C_p is the power coefficient.

For the tidal turbine's efficiency, it can be known basically by conducting the power coefficient times 100% as below:

$$\eta = C_p \times 100\% \quad (4)$$

where η is a tidal turbine efficiency.

Reynolds-Average Navier-Stokes Equation (RANS)

The RANS model is an equation that calculates the average flow of an incompressible fluid. When compared to Large Eddy Simulation, RANS simulation will have a shorter simulation time (LES). The steady-state RANS formulation is shown in Equation (1).

$$\rho \frac{\partial \overline{u_i}}{\partial t} + \rho \overline{u_j} \frac{\partial \overline{u_i}}{\partial x_j} = -\frac{\partial \bar{p}}{\partial x_i} + \frac{\partial}{\partial x_j} (\mu \frac{\overline{u_i}}{\partial x_j} - \rho \overline{u_{i'} u_{j'}}) \quad (5)$$

where $\bar{p}$ is time-averaged relative pressure, $-\rho \overline{u_{i'} u_{j'}}$ is the Reynolds stress tensor, ρ is the liquid density, and μ is the liquid's dynamic viscosity.

Standard k-epsilon Model

In any flow simulation, a standard k-epsilon model is typically used for turbulent modelling. It is a strong and reliable equation that can be applied to a wide range of engineering problems and also can produce accurate simulation results while using less computational power. The transportation equation for k and ε is given below.

$$\frac{\partial}{\partial x_i}(\rho k u\bar{i}) = \frac{\partial}{\partial x_j}\left[\left(\mu + \frac{\mu_t}{\sigma_k}\right)\frac{\partial \varepsilon}{\partial x_j}\right] + G_k - Y_k \quad (6)$$

$$\frac{\partial}{\partial x_i}(\rho k u\bar{i}) = \frac{\partial}{\partial x_j}\left[\left(\mu + \frac{\mu_t}{\sigma_\varepsilon}\right)\frac{\partial \varepsilon}{\partial x_j}\right] + G_\varepsilon - Y_\varepsilon \quad (7)$$

Where k is the turbulent kinetic and ε turbulent dissipation, μt is the eddy viscosity. Equations (2) and (3) show the turbulent Prandtl number which is the σ_k and σ_ε

RESULT AND DISCUSSION

The outcome of the simulation is significant since it demonstrates how the velocity contour evolves over the area. This makes the result relevant, the velocity contour may be used to determine the wakes that are produced as well as the features of the wakes, such as whether the wake is near or far away. The wake that is produced may be used to calculate the rate at which wake recovery happens from upstream to downstream throughout the domain. The sooner the wake recovers after the turbine, the less turbulence and shear stress profile will be formed downstream of the domain.

The research is interested in the evolution of the velocity contour over the region. The wake created may be recognized and its characteristics such as close and distant wakes can also be seen using the velocity contour. The wake created may show if the domain's wake recovery is rapid or sluggish. Additionally, the research is interested in the theoretical efficiency of energy conversion inside the tidal farm. The theoretical findings will briefly describe the tidal farm's performance.

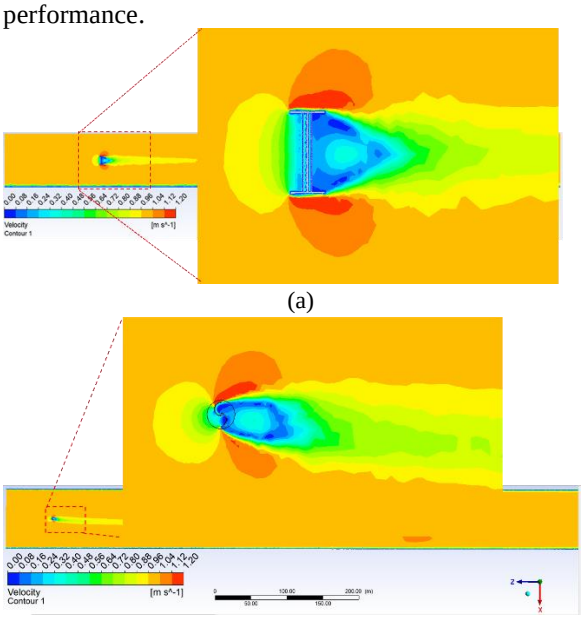

(a)

(b)

Figure 7 Velocity contour of Savonius turbine. (a) Side view of domain; (b) Top view of the domain

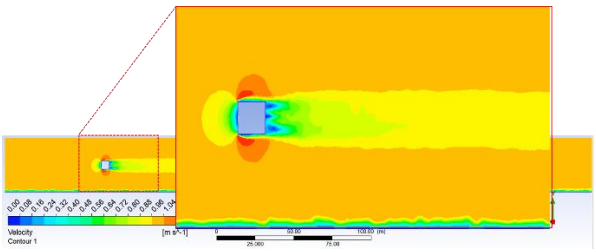

Fig 8 Velocity contour of cylinder

Figure 7 shows the velocity contour for a Savonius turbine single stage. The turbine has the greatest deceleration upstream, as seen from the side. The wake deceleration for a single turbine may be observed fully downstream of the rotor from the velocity wake contour measurement. Similarly, Figure 8 shows the velocity contour of a cylindrical object.

The velocity curve of a single-stage Savonius turbine at 1.0 m/s is shown in Figure 7. The red counter in the figure represents the energy received from the flow after it passes through the turbine. The single-stage turbine also generates more energy and as seen in Figure 7, has a swing wake flow in the downstream zone because of the curve blade that affects the wake flow when viewed from the top. It was discovered from the velocity contour that the momentum of the upstream flow increased as it got closer to the advancing blade as demonstrated by Nauman Riyaz Maldar [15].

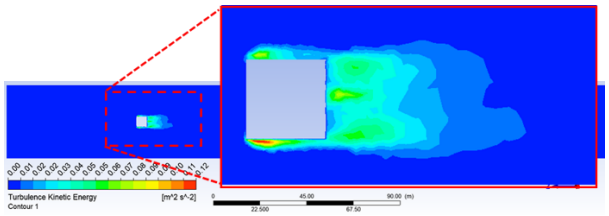

(a)

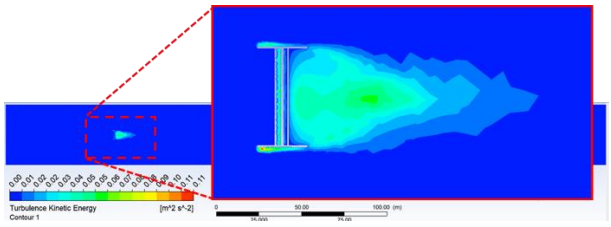

(b)

Fig 9 (a) Turbulence kinetic energy contour of a hypothetical cylinder from a side view at YZ plane; (b) Turbulence kinetic energy contour of Savonius turbine from a side view at YZ plane.

Figure 9 illustrates, for a Savonius turbine and a hypothetical cylinder of boundary conditions, the contour for turbulence kinetic energy on the YZ plane produced from the CFD simulation. The findings indicate that there is a significant level of turbulent kinetic energy near the bottom of both kinds of models, which is around 0.11 m^2/s^2.

MULTI-ROW STAGGERED ARRAY CONFIGURATION

In addition, since the average velocity in the wake is less than the velocity of the free stream, the velocity outside the wake in a closed channel must be a substantial amount higher than the free stream to preserve the continuity of the volume and flow rate. As a direct consequence of the blocking effect, the flow is enhanced around the Savonius tidal current turbine. Figure 10 shows the velocity contour of a two-rows array. Figure 11 shows the first row of turbines in a multi-row array introduce turbulence into the flow, which affects the hydrodynamics of the successive rows downstream. In the case of the staggered configuration, the blue zone of the rotor that is in the first row has an immediate and decisive impact on the rotor that is located downstream.

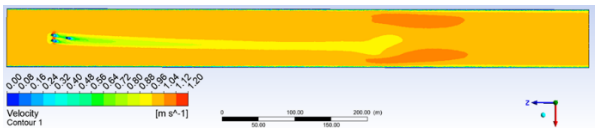

(a)

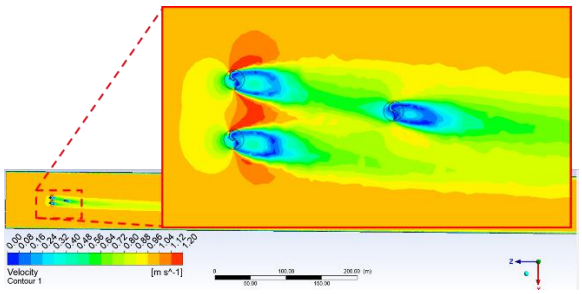

Fig 10 Velocity contour of Savonius turbine. (a) Side view of domain; (b) Top view of the domain

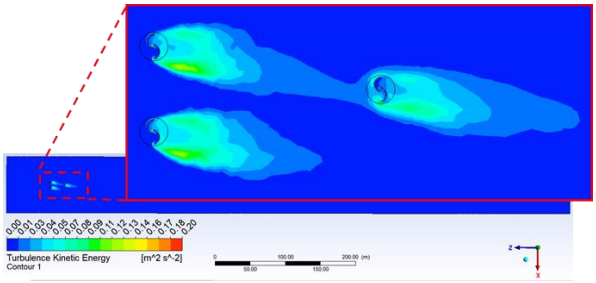

Fig 11 Turbulence kinetic energy of a two-rows array from top view at ZX plane.

Figure 12 shows the experimental data at 8D, 10D and 12D downstream. As illustrated in the figure, some

comparisons involved the simulation for velocity deficit between staggered array, inline and single Savonius model. For the staggered array model, the plotting has higher at 8D downstream between inline setup and single setup. Figure 13 then shows the turbulence intensity for sliding mesh simulation. The three graphs indicate the same pattern, with moderate turbulence intensity for inline and single setup of Savonius turbine for 8D, 10D and 12D. Although the trend in this data for stagged setup is lowest at 8D downstream, it is greater at 10D and 12D downstream. The 8D downstream is too little, and the value is too small.

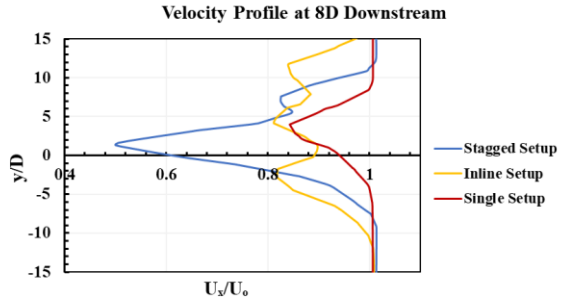

(a)

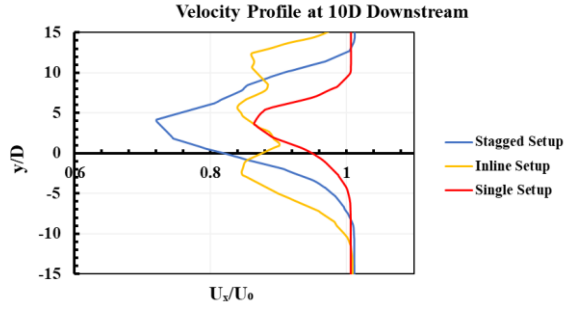

(b)

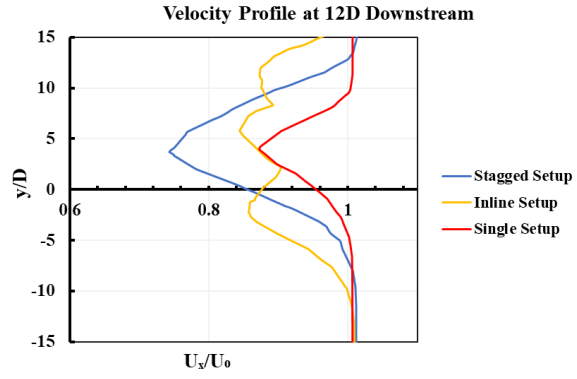

(c)

Fig 12 Velocity deficit of the turbine configuration. (a) Velocity Profile at 8D Downstream; (b) Velocity Profile at 10D Downstream; (c) Velocity Profile at 12D Downstream

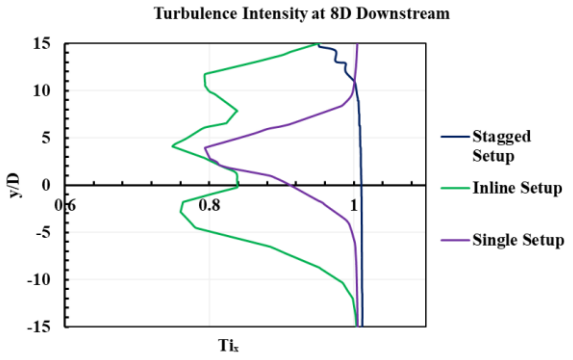

(a)

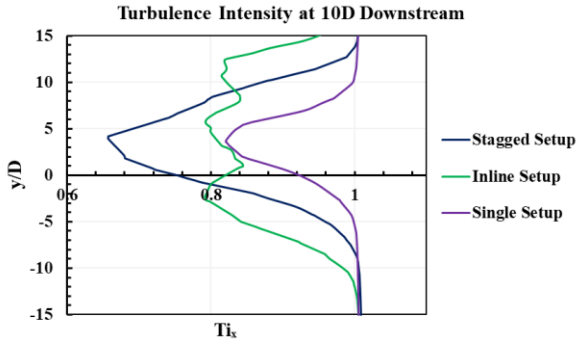

(b)

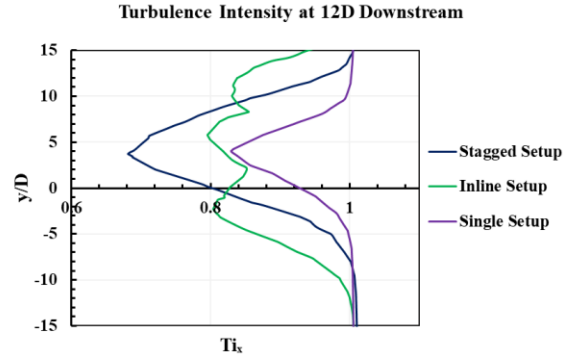

(c)

Fig 13 Turbulence intensity of the turbine configuration. (a) Turbulence intensity at 8D Downstream; (b) Turbulence intensity at 10D Downstream; (c) Turbulence intensity at 12D Downstream.

One of the many methods that can be used to compare predictions is the mean absolute error. Table 9 shows the mean absolute error of multi-row simulations comparison in velocity magnitude and turbulence intensity.

Table 9 Mean absolute error of multi-row stagged array

Comparison of Absolute Error	Mean Absolute error

Multi-Row Staggered Array	Velocity Magnitude	8D Staggered	9.1655
		8D Inline	6.9582
		10D Staggered	6.0759
		10D Inline	6.1873
		12D Staggered	5.7696
		12D Inline	6.0058

SINGLE ROW OF THREE TURBINES CONFIGURATION

Because the installation of arrays in a single row produces fewer effective results when applied over a large area, the emphasis of this research will be placed on shallow water applications. The mesh refinement used for the three turbines simulation was the same as that applied to the single turbine simulation that was completed and discussed in the sections before this one. A single-row layout scheme is selected for the multi-rotor turbine array.

Figures 14 shows the flow past a single row of three turbines with a lateral hub to hub spacing of 1.5D, as well as the velocity and turbulence intensity contour computed with the fine mesh 2.0m. The velocity distribution suggests that after the approach flow encounters the turbines, it accelerates on the side and top view of the row and between the turbines, as the compact spacing between them favours the user-specified blockage, resulting in a high-velocity bypass flow between them. High levels of turbulence kinetic energy in the same spot as a single turbine are found in the back rotor area and in the wake extension over which tip vortices travel coherently, as shown in Figure 15.

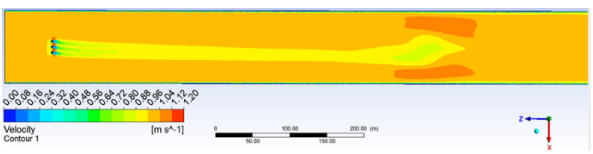

(a)

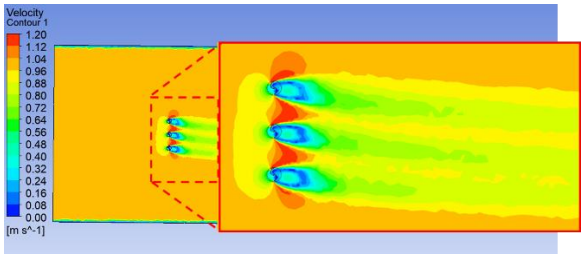

(b)

Fig 14 Velocity Contour of Inline Array. (a) Top views slices at ZX plane of the velocity contour; (b) Close-up view velocity wake of the turbine

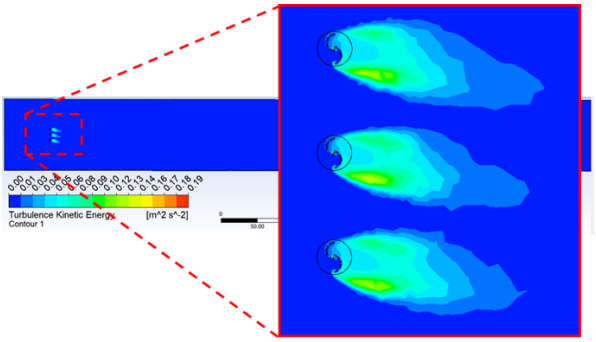

Fig 15 Turbulence kinetic energy of inline array from top view at ZX plane

The experimental data extracted from the Stallard et al [16] was used to determine if it was suitable to finish the arrangement on a single-row inline. As depicted in Figure 16, at 8D,10D and 12D, there are differences between the Savonius model inline setup and the experimental data values. The power generation of the tidal turbine is known to be affected by the turbulence intensity of the incoming flow. The intensity of the turbulent flow is essentially consistent across the water depth at each cross-section. As a result, the rate of momentum recovery is anticipated to diminish as downstream distance rises, as seen in figure 17.

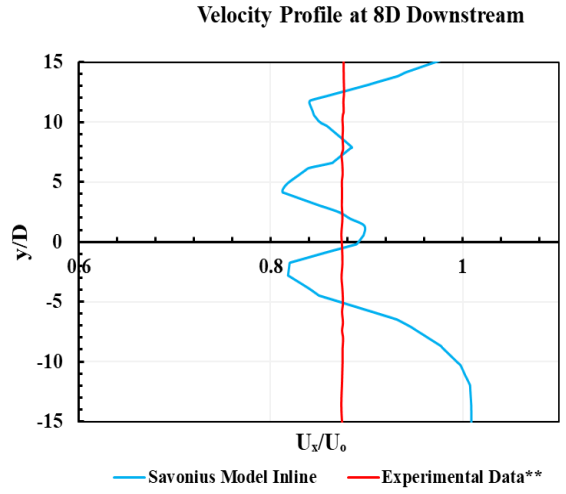

(a)

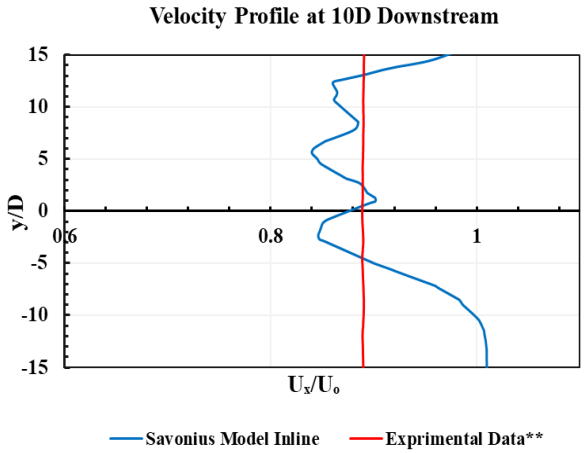

(b)

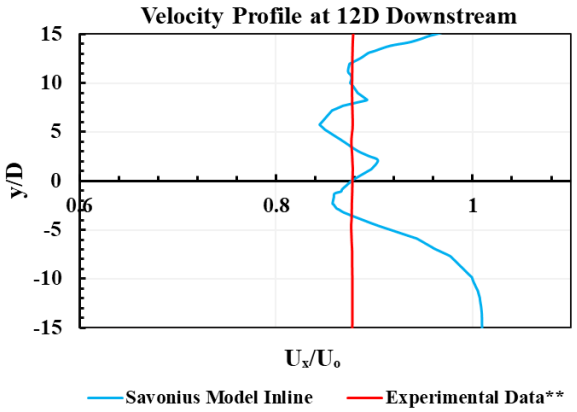

(c)

Fig 16 Velocity deficit at different downstream of a row of three turbines with 1.5D lateral spacing. (a) Velocity Profile at 8D downstream; (b) Velocity Profile at 10D downstream; (c) Velocity Profile at 12D downstream

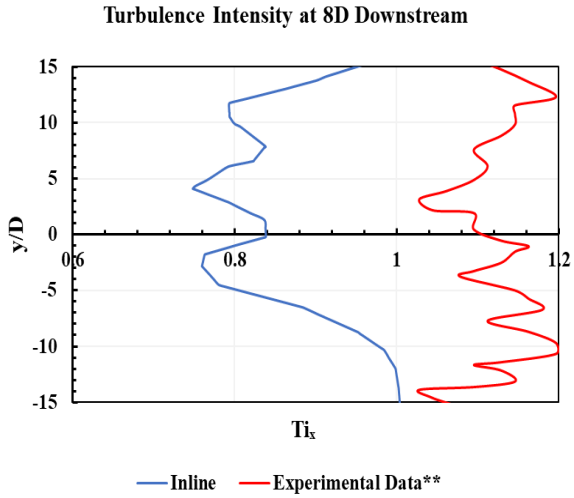

(a)

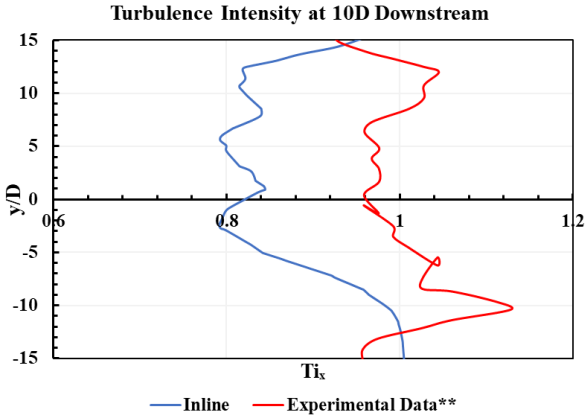

(b)

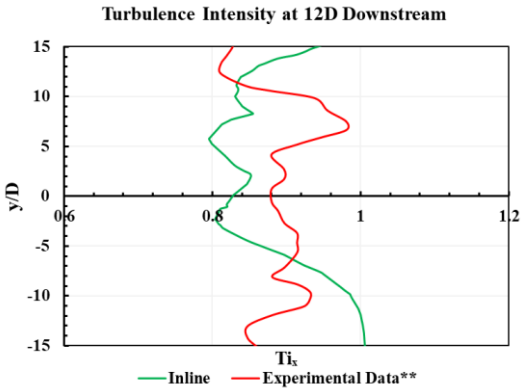

(c)

Fig 17 Turbulence intensity at different downstream of a row of three turbines with 1.5D lateral spacing. (a) Turbulence intensity at 8D downstream; (b) Turbulence intensity at 10D downstream; (c) Turbulence intensity at 12D downstream

One of the many methods that may be used to compare predictions is the mean absolute error. Table 10 shows the mean absolute error of multi-row simulations comparison in velocity magnitude and turbulence intensity. The number of error points taken is 60 points for every graph plot in the single-row array result.

Table 10 Mean Absolute error of Single-row array

Comparison between Simulation and Paper Validation			Mean Absolute error
Single-Row Array	Velocity Magnitude	8D	5.4916
		10D	4.8046
		12D	4.9695

CONCLUSION

The primary objective of this study is to determine the problems caused by the VATT which is currently used in shallow water situations. The CDF simulation was used to evaluate the performance of the Savonius turbine design under static circumstances. The results of the research and studies served as the basis for this inquiry (CFD). This project has been examined by displaying numerous different forms of refinement based on the data that were found. The finding led to the conclusion that the refinement of the mesh is of a greater grade compared to the prior settings. In addition, selecting an axis point might be challenging due to the layout of the components.

A comparison of the wake interaction of the Savonius turbine design with a cylindrical object that symbolizes VATT was discussed in this paper. As a direct consequence of this research, an investigation was carried out into the interaction between a Savonius turbine with a cylindrical object regarding the velocity wake. The results that have been obtained from this study which velocity contour and turbulence kinetic energy for single setup, multi-row setup and single-row three turbine setup. When opposed to an actuator cylinder that is designed to seem like a turbine, using a design that is based on a real Savonius turbine offers a higher level of detail and accuracy.

In conclusion, the findings on the quantitative data regarding the mean absolute error had been identified in the result, and there are percentages on the comparison graph plot of the graph plotting velocity magnitude and turbulence intensity. It is logically acknowledged that the average value of mean absolute is less than 10% of the value percentages that have been obtained. Therefore, there is not much of a difference when comparing the outcomes of simulations with those of paper validations of experimental data.

ACKNOWLEDGMENTS

The authors gratefully acknowledge the financial The authors gratefully acknowledge the support received from the Ministry of Higher Education Malaysia through the Fundamental Research Grant Scheme for Research Acculturation of Early Career Researchers (FRGSRACER) RACER /1/2019/TK07/UNIMAP/1. Additionally, the authors are also thankful for the support received from Universiti Malaysia Perlis, specifically from the Research Management Centre (RMC).

REFERENCES

[1] F. S. Mohd Chachuli, S. Mat, N. A. Ludin, and K. Sopian, “Performance evaluation of renewable energy R&D activities in Malaysia,” Renewable Energy, vol. 163, pp. 544–560, Jan. 2021, doi: 10.1016/j.renene.2020.08.160.

[2] S. M. C. Fairuz et al., “Long term strategy for electricity generation in Peninsular Malaysia - Analysis of cost and carbon footprint using MESSAGE,” Energy Policy, vol. 62, pp. 493–502, Nov. 2013, doi: 10.1016/j.enpol.2013.08.005.

[3] M. Davis, A. Moronkeji, M. Ahiduzzaman, and A. Kumar, “Assessment of renewable energy transition pathways for a fossil fuel-dependent electricity-producing jurisdiction,” Energy for Sustainable Development, vol. 59, pp. 243–261, Dec. 2020, doi: 10.1016/j.esd.2020.10.011.

[4] S. Özgül, G. Koçar, and A. Eryaşar, “The progress, challenges, and opportunities of renewable energy cooperatives in Turkey,” Energy for Sustainable Development, vol. 59, pp. 107–119, Dec. 2020, doi: 10.1016/j.esd.2020.09.005.

[5] “Malaysia aims 31% RE capacity by 2025 - MIDA | Malaysian Investment Development Authority.” https://www.mida.gov.my/mida-news/malaysia-aims-31-re-capacity-by-2025/ (accessed Nov. 14, 2021).

[6] T. Husseini, “Tidal energy advantages and disadvantages: key points to consider,” Power Technology, Oct. 26, 2018. https://www.power-technology.com/features/tidal-energy-advantages-and-disadvantages/ (accessed Jan. 24, 2022).

[7] P. A. J. Bonar, A. M. Schnabl, W. K. Lee, and T. A. A. Adcock, “Assessment of the Malaysian tidal

Stream Energy resource using an upper bound approach," Journal of Ocean Engineering and Marine Energy, vol. 4, no. 2, pp. 99–109, May 2018, doi: 10.1007/s40722-018-0110-5.

[8] W. S. W. Abdullah, M. Osman, M. Z. A. A. Kadir, and R. Verayiah, "The potential and status of renewable energy development in Malaysia," Energies (Basel), vol. 12, no. 12, 2019, doi: 10.3390/en12122437.

[9] Y.P. Cai, H. Huang, S.C. Yeh, L. Liu, C. Li, "A modelling approach for investigating climate change impacts on renewable energy utilization.," Int J Energy Res, vol. 3, no. 6, pp. 764–722, May 2012.

[10] W. S. W. Abdullah, M. Osman, M. Z. A. A. Kadir, and R. Verayiah, "The potential and status of renewable energy development in Malaysia," Energies (Basel), vol. 12, no. 12, 2019, doi: 10.3390/en12122437.

[11] Anaa Lavaa, "Tidal Energy Diagram: The Story of Tidal Power Based on Diagrams - Industrial Manufacturing Blog | linquip," Linquip Technews, Feb. 06, 2021. https://www.linquip.com/blog/tidal-energy-diagram-story-of-tidal-power/ (accessed Jan. 24, 2022).

[12] Suhri, G. E., Rahman, A. A., Dass, L., Rajendran, K., & Rahman, A. A. (2022). Interactions Between Tidal Turbine Wakes: Numerical Study for Shallow Water Application. Jurnal Teknologi, 84(4), 91-101.

[13] Qing'an, L., Yasunari, K., Takao, M., Junsuke, M. and Yusuke, N. 2016. Visualization of the flow field and aerodynamic force on a Horizontal Axis Wind Turbine in turbulent inflows. Energy 111, 57-67.

[14] Meng-Hsien, L., Shiah, Y.C. and Chi-Jeng, B. 2016. Experiments and numerical simulations of the rotor-blade performance for a small-scale horizontal axis wind turbine. J Wind Eng Ind Aerodyn 149, 17-29.

[15] N. R. Maldar, C. Y. Ng, and E. Oguz, "A review of the optimization studies for Savonius turbine considering hydrokinetic applications," Energy Conversion and Management, vol. 226. Elsevier Ltd, Dec. 15, 2020. doi: 10.1016/j.enconman.2020.113495.

[16] T. Stallard, R. Collings, T. Feng, and J. Whelan, "Interactions between tidal turbine wakes: Experimental study of a group of three-bladed rotors," Philosophical Transactions of the Royal Society A: Mathematical, Physical and Engineering Sciences, vol. 371, no. 1985, Feb. 2013, doi: 10.1098/rsta.2012.0159.